Title

Real-time cavitation monitoring during optical coherence tomography guided photo-mediated ultrasound therapy of the retina

Journal

IEEE Transactions on Biomedical Engineering, PP(99)

ISSN

0018-9294

Authors

Wang, Mingyang
Zhang, Wei
Chen, Zhongping
et al.

Publication Date

2024-03-18

DOI

10.1109/tbme.2024.3377115

Real-time cavitation monitoring during optical coherence tomography guided photo-mediated ultrasound therapy of the retina

Mingyang Wang, Wei Zhang, Zhongping Chen, Yannis M. Paulus, Xueding Wang, and Xinmai Yang*

Abstract* — *Objective: **Photo-mediated ultrasound therapy (PUT) is a novel antivascular therapeutic modality based on cavitation-induced bioeffects. During PUT, synergistic combinations of laser pulses and ultrasound bursts are used to remove the targeted microvessels selectively and precisely without harming nearby tissue. In the current study, an integrated system combining PUT and spectral domain optical coherence tomography (SD-OCT) was developed, where the SD-OCT system was used to guide PUT by detecting cavitation in real time in the retina of the eye. *Method:* We first examined the capability of SD-OCT in detecting cavitation on a vascular-mimicking phantom and compared the results with those from a passive cavitation detector. The performance of the integrated system in treatment of choroidal microvessels was then evaluated in rabbit eyes *in vivo*. *Results:* During the *in vivo* PUT experiments, several biomarkers at the subretinal layer in the rabbit eye were identified on OCT images. The findings indicate that, by evaluating biomarkers of treatment effect, real-time SD-OCT monitoring could help to avoid micro-hemorrhage, which is a potential major side effect. *Conclusion:* Real-time OCT monitoring can thus improve the safety and efficiency of PUT in removing the retinal and choroidal microvasculature.**

***Index Terms*— angiogenesis; image guided treatment; laser; optical coherence tomography; photo-mediated ultrasound therapy; retina**

I. Introduction

Acoustic cavitation has played an important role in a remarkable range of medical procedures such as tumor ablation [1], tissue emulsification [2], and drug delivery [3]. The acoustic cavitation process involves the storage of the acoustical energy by the liquid system in what is called the growth phase and the ultimately focused release of the acoustical energy during the collapse phase [4]. During the spatiotemporally focused release of energy, several mechanical and chemical effects [4], including microstreaming [5], microjets [6], shock waves [7], and free radical formation [8], can be produced. These mechanisms in turn lead to a list of bioeffects such as improving cell permeabilization [9], inducing cell necrosis [10], regulating gene expression [11], improving cell proliferation [12], and changing cell viability [13], leading to the desired therapeutic outcomes as a result of acoustic cavitation during the aforementioned medical procedures.

Photo-mediated ultrasound therapy (PUT) is an emerging antivascular therapy technique that relies on cavitation-induced bioeffects [14]. By using a synergistic combination of laser pulses and ultrasound bursts, PUT can remove the targeted microvessels with no or minimized damage to the surrounding tissue. The efficacy of PUT has been investigated and evaluated in various disease models *in vivo*, including corneal neovascularization [15], retinal neovascularization [16], choroidal neovascularization [17], and hypervascularity skin model [18, 19]. In these studies, as a general procedure, the applied laser and ultrasound parameters were first titrated on several animals, then the optimized values were used in the following PUT experiments for efficacy evaluation, while the treatment duration was fixed for each experiment. However, due to biological variations, a fixed treatment duration can cause over- or under-treatment, resulting in either excessive side effects, such as microhemorrhage, or unachieved treatment outcome. To improve the safety (by avoiding over-treatment) and efficacy (by avoiding under-treatment), which are particularly crucial for performing PUT at the highly sensitive retinal and choroid layers in the eye, personalized treatment based on some real-time feedback is desirable.

Because PUT is based on acoustic cavitation, it is imperative to monitor the cavitation activity during PUT in order to provide real-time feedback. Passive cavitation detection (PCD) is a widely used acoustic approach to detect acoustic cavitation. The use of PCD has brought major advances to our understanding of cavitation dynamics and associated bioeffects by detecting cavitation noise emitted by cavitation bubbles [20]. Studies have found a substantial correlation between cavitation intensity and cavitation noise[21]. While cavitation noise is highly complicated, broadband noise is frequently thought to be caused by inertial cavitation[22]. Therefore, studies have used the cavitation noise spectral integral as a criterion to assess inertial cavitation activity[23].

Manuscript submitted on 19 July 2023 for review. This study is supported in part by NIH 1R01EY029489 (XY), NIH 1K08EY027458 (YMP), NIH 1R41EY031219 (YMP), the Alliance for Vision Research (YMP), the Alcon Research Institute Young Investigator Grant (YMP), and unrestricted departmental support from Research to Prevent Blindness (YMP). This work utilized the Vision Research Core Center funded by P30EY007003 from the National Eye Institute. (Corresponding author: Xinmai Yang.)

Mingyang Wang is with University of Michigan, Ann Arbor, MI, USA. Wei Zhang is with University of Michigan, Ann Arbor, MI, USA. Zhongping Chen is with University of California Irvine, Irvine, CA 92617, USA. Yannis M. Paulus is with University of Michigan, Ann Arbor, MI, USA. Xueding Wang is with University of Michigan, Ann Arbor, MI, USA. Xinmai Yang is with University of Kansas, Lawrence, KS, 66045, USA (correspondence e-mail: xmyang@ku.edu).

Conventional PCD using a single-element transducer has a spatially dependent sensitivity. Moreover, due to its poor spatial resolution, PCD based on a single-element transducer is unable to separate the mixture of acoustic emission it receives from multiple source locations [24, 25]. As a result, it is very difficult to use PCD to detect cavitation activity in single microvessels in the fundus of the eye. In addition to cavitation detection, real-time assessment of the structure of the microvessels treated by PUT is also important to avoid potential overtreatment. Hence, a modality suitable for both bubble detection and structure detection holds promise to contribute to personalized PUT treatment of microvessels at the fundus of the eye.

Optical coherence tomography (OCT) is a technique capable of both anterior and posterior segment imaging of human eyes with micrometer-scale spatial resolution, enabling superior delineation of ocular morphology and highly precise biometry [26, 27]. Since the first OCT system was developed, the modality has advanced rapidly. Studies have shown that swept source OCT (ss-OCT) can provide an A-scan at a rate greater than 100 kHz [28, 29]. At this rate, high-resolution images of dynamic events can be captured and displayed in real time in clinical applications such as refractive corneal surgery [30], glaucoma assessment [31], and subretinal injection [32]. A recent study demonstrated the feasibility of using OCT angiography (OCTA) to guide a high speed PUT system for real-time detection of vessel changes in a rabbit ear model [33]. However, cavitation formation, which is the mechanism responsible for the bioeffect of PUT, has not been detected *in vivo*. Detecting cavitation formation during PUT can potentially predict vessel response in an early stage.

In this study, we examined the feasibility of using OCT for real-time monitoring of the cavitation formation in microvessels of the fundus in the eye during PUT treatment. We developed a system that combined a PUT system with a spectral domain OCT (SD-OCT) which allows OCT and PUT to be performed simultaneously in the same eye. The capability of the SD-OCT in detecting cavitation activity was first investigated on a vascular-mimicking phantom, and the results were compared to those from PCD. Then the feasibility of SD-OCT in guiding PUT treatment of the choroidal microvessels was investigated in a clinically relevant rabbit eye model *in vivo*. Our study demonstrated that the integrated SD-OCT and PUT system could improve the safety and efficacy of PUT by visualizing the cross-section of the fundus of the eye in real time and predicting the treatment outcome.

II. METHOD

A. PHANTOM STUDY

1) System components

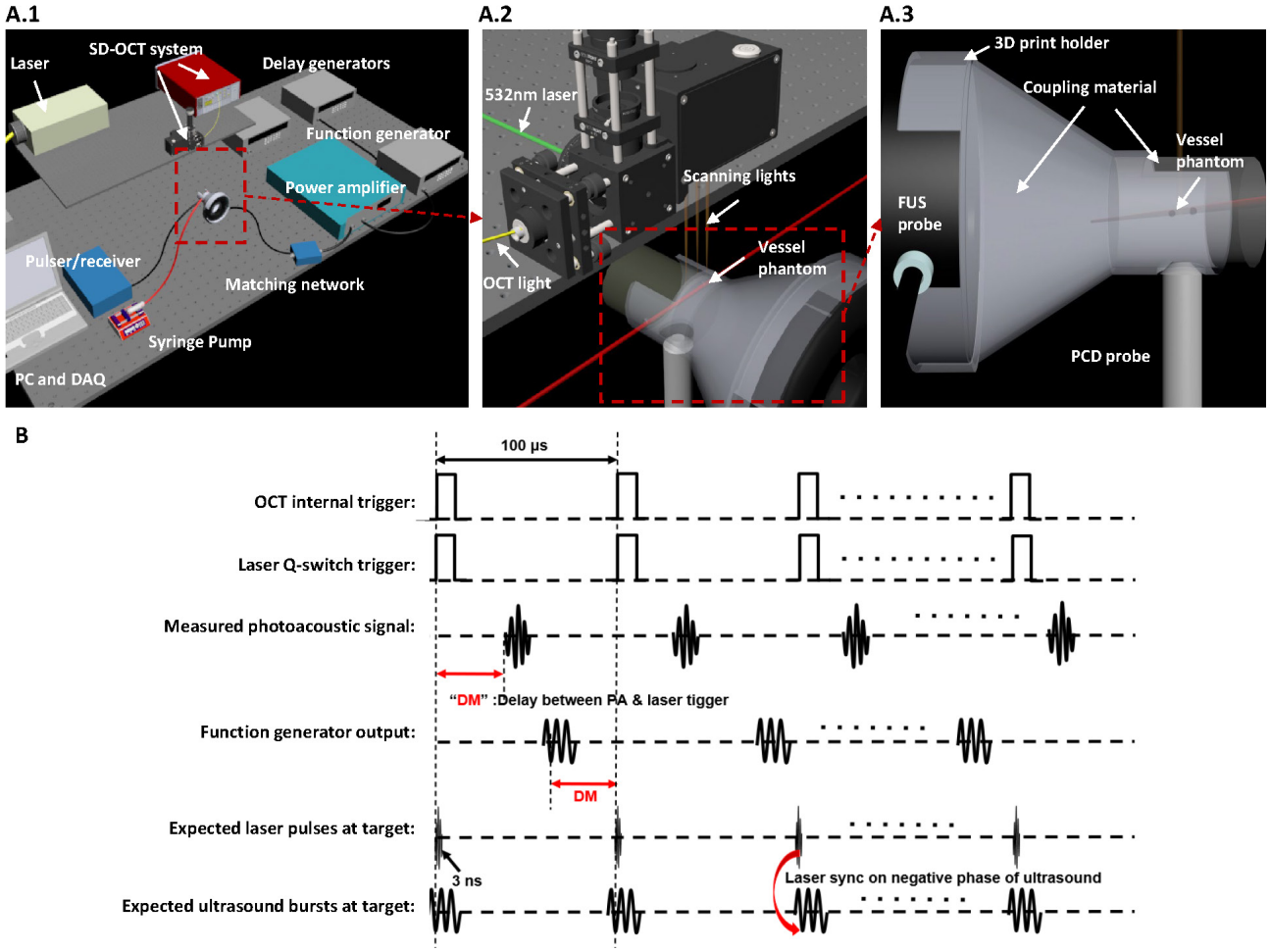

Fig. 1. System schematic and timing sequence for the phantom study. (A.1) The integrated PUT and SD-OCT system. (A.2) Side view of optical alignment, the 532nm and OCT light share focus and scanning along the vessel phantom. (A.3) Side view of the acoustic alignment, The PCD was positioned to confocal with the FUS transducer aiming at the vessel phantom at a 90° angle. (B) Time sequence for system synchronization.

A schematic of the newly developed integrated PUT and SD-OCT system is shown in Fig.1-A. In PUT, a 0.25 MHz focused ultrasound (FUS) transducer with a focal width of 6.04 mm and a focal length of 39.49 mm (H-117, Sonic Concepts, Bothell, WA, USA) was driven by a power amplifier (2100L, Electronics & Innovation Ltd, Rochester, NY, USA) via an impedance matching network. The focal pressure of the FUS transducer was calibrated in situ by using a standard needle hydrophone (HNC-1000, Onda Corporation, Sunnyvale, CA, USA) [34]. The therapeutic light for PUT was supplied by a 532-nm fiber laser (GLPN-M, IPG Photonics, MA, USA) with tunable repetition rate and 1.5-ns pulse duration. The SD-OCT was adapted from a commercially available OCT platform (TEL321C1, Thorlabs, NJ, USA). The two laser beams for PUT and OCT were coaxially aligned through a dichroic mirror (FF925-Di01-25x36, Semrock, IDEX Health & Science, NY, USA) before entering the galvanometer scanning system (OCTP 1300, Thorlabs). The combined laser beam was delivered and focused on the same area through a scan lens (LSM-03, Thorlabs) by sharing the same galvanometer [35].

A vascular mimicking phantom was created by embedding a silicone tube (inner diameter: 0.3 mm; outer diameter: 0.6 mm, Liveo™ Silicone Laboratory Tubing, Fisher Scientific) in a coupling gel material, which was made by mixing porcine gelatin powder in boiling water at a 1:10 ratio in weight. To mimic the blood flow in human choroidal vessels, the tube was filled with human whole blood, and the blood was circulated by a syringe pump at a speed of 1 cm/s [36]. PCD was used to confirm inertial cavitation activity in the blood flow. To detect cavitation activity through PCD, a focused immersion ultrasound transducer with a center frequency of 10 MHz (V312, Olympus, Tokyo, Japan) was used, and its focus overlaid the FUS focal area, which was targeted on the vessel. The cavitation signal detected by PCD was first amplified by a pulser/receiver (5072PR, Olympus, Tokyo, Japan) and then digitized by a DAQ card (RazorMax, Gage) with a sampling rate at 125 MHz. The phantom vessel was also scanned by the B-mode SD-OCT along the longitudinal axis

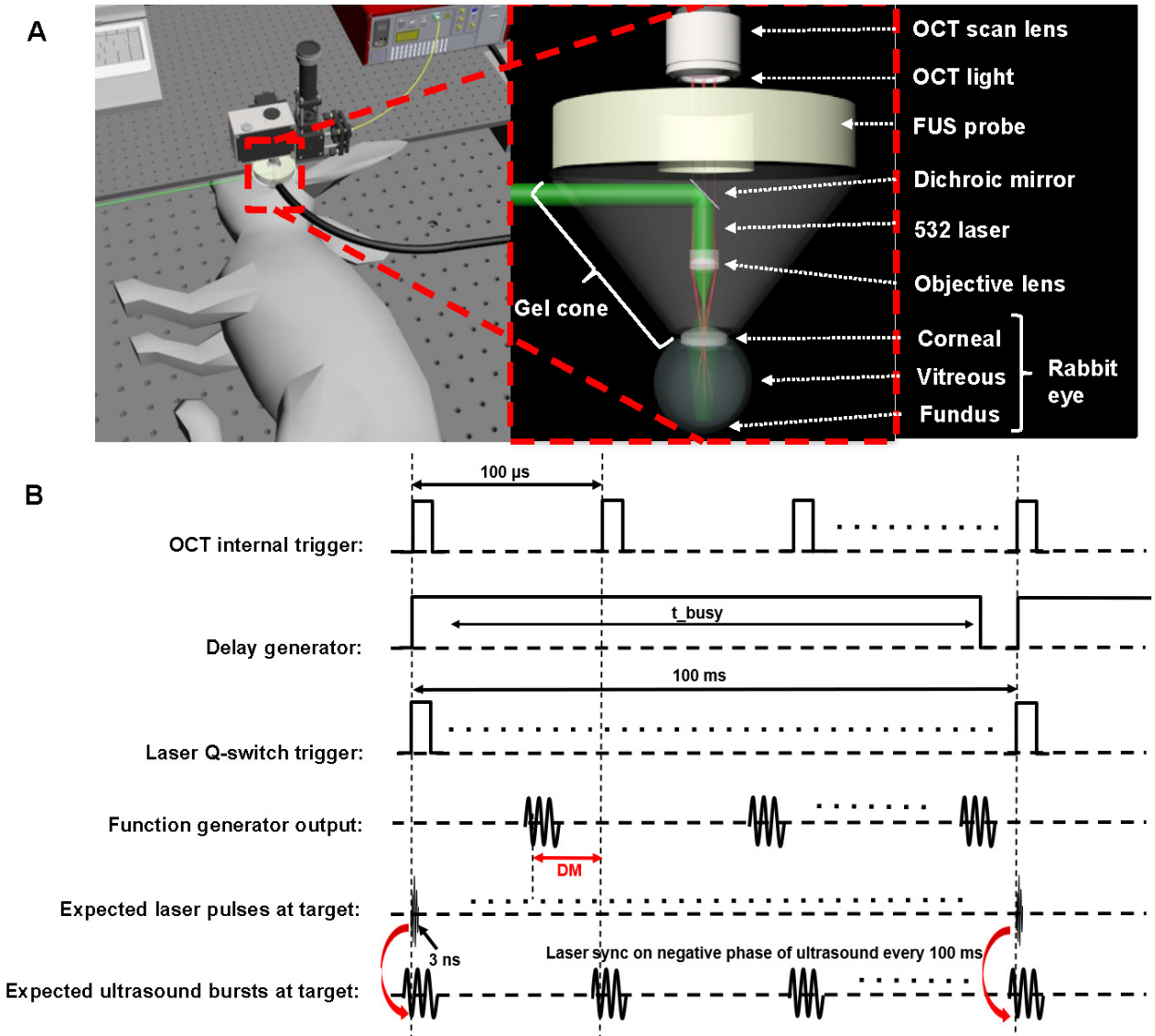

Fig. 2. System schematic and timing sequence for the study on rabbit eye *in vivo*. (A) The combined FUS, OPO laser, and OCT system. (B) Timing sequence for synchronization of devices. DM: delay time measurement.

with a real-time display. The SD-OCT provides a lateral resolution of 13 μm and an axial resolution of 4.2 μm. With this arrangement, the cavitation signal from the same region of the vessel phantom was simultaneously detected by PCD and SD-OCT.

2) Synchronization of the integrated system

The timing sequence of the integrated system was precisely controlled by a pulse delay generator (DG535, Stanford Research Systems) as shown in Fig.1-B. The internal trigger signal from the SD-OCT system with a 10 kHz pulse repetition rate was used to precisely trigger the fiber laser, the FUS system, and the DAQ card. The pre-trigger delay for FUS signal was set based on the ultrasound traveling time from the FUS probe to the target. To measure this traveling time, the FUS probe was initially used in receiving mode, whereas the 532 nm laser was used to generate photoacoustic (PA) signal from the blood vessel phantom. The measured delay between the laser trigger and the FUS detected PA signal, which is the traveling time labeled as DM in Fig.1-B, was precisely calculated and applied to the function generator of the FUS system via the pulse delay generator. As a result of the synchronization described in Fig.1-B, the laser pulse was anticipated to irradiate the blood vessel when the negative phase of the FUS burst also reached the blood vessel.[37]

3) Phantom study data collection

Eight different laser energy levels for PUT was used, evenly spreading from 0 to 1.4 μJ/pulse with a beam diameter around 10 μm. The FUS peak negative pressure at the target was also set to 8 different levels by adjusting the function generator output voltage, evenly distributing from 0.156 to 0.228 MPa. As a result, the targeted vessel was treated by a total of 64 combinations of different laser pulse energy levels and FUS pressure levels. The PCD signal, which was digitized by the DAQ card, was simultaneously recorded during the SD-OCT B-scan with a time duration of 100 OCT B-scan frames (512×100 A-scans). The power spectrum of the captured PCD signal was then calculated for further analysis.

B. IN-VIVO STUDY

1) System components for in vivo study

To validate the performance of real-time OCT guidance during PUT treatment of rabbit eyes *in vivo*, the system was further upgraded to accommodate the rabbit eye. A high-power mobile laser (Phocus Mobile, Opotek, CA, USA) was used to replace the fiber laser that has been used in the *in vitro* study on phantoms. The high-power laser system can supply a beam of larger size on the fundus at the desired light fluence. The wavelength was tuned to 532 nm which is an isosbestic point of oxygenated hemoglobin and deoxygenated hemoglobin and has been demonstrated effective for selectively treating blood vessels in the eye using PUT [38]. A conical-shape gel cone was used to provide coupling for ultrasound propagation from the FUS transducer to the eye surface. As shown in Fig.2-A, there were holes in the gel cone to provide optical paths for both PUT and OCT laser beams. The laser beam for PUT propagated through the side hole and was reflected by a dichroic mirror (FF925-Di01, Semrock, IDEX Health & Science, NY, USA) in the middle hole to align with the acoustic beam. The OCT light coming out of the scan lens (LSM03, Thorlabs, NJ, USA) passed through the same dichroic mirror in the middle hole and was then collimated with the PUT light beam by the ophthalmic lens (AC080-010-C-ML, Thorlabs) before entering the eye. A custom-made 3D-printed lens holder was used inside the middle hole to hold all the optical components.

2) Synchronization of the in vivo treatment monitoring system

Fig.2-B depicts the timing sequence used to synchronize different devices in the *in vivo* setup. The entire system was triggered by the OCT internal trigger signal operating at 10 kHz, and 0.25 MHz FUS transducer produced three-cycle pulses at a 10 kHz pulse repetition rate. One of the channels from pulse delay generator was set to trigger holdoff mode to generate 10 Hz output trigger signals for the laser system. The treatment laser pulse energy was precisely controlled by adjusting the delay between the Q-switch and the flashlamp. The delay between the treatment laser Q-switch and the FUS system was adjusted by the aforementioned method based on the PA signal to ensure that each laser pulse reached the target at the same time as the negative peak of a FUS pulse arrived. Because FUS had a pulse repetition rate of 10 kHz while the laser system ran at 10 Hz, combined FUS and laser irradiation only occurred once every 1000 FUS pulses.

3) Animal handling and treatment procedure

Eleven New Zealand white rabbits, acquired from the Center for Advanced Models and Translational Sciences and Therapeutics at the University of Michigan Medical School, participated in this study to investigate the OCT biomarkers caused by cavitation bubbles during PUT treatment. All the experimental procedures were performed in accordance with the ARVO (The Association for Research in Vision and Ophthalmology) Statement for the Use of Animals in Ophthalmic and Vision Research and were approved by the Institutional Animal Care & Use Committee (IACUC) of the University of Michigan (Protocol PRO00010387, PI: Yannis Paulus). The rabbits were anesthetized by intramuscular injection with a mixture of Ketamine (40 mg/kg, 100 mg/mL) and Xylazine (5 mg/kg, 100 mg/mL). One drop of 2.5% phenylephrine hydrochloride and one drop of 1% tropicamide were used to dilate the pupil. Prior to treatment, 0.5% ophthalmic tetracaine was applied to provide topical anesthetic. The rabbit vital signs, including mucous membrane color, temperature, heart rate, respiratory rate, and oxygen saturation, were observed every 15 minutes during the entire procedure.

During PUT procedure, the first five rabbits were used to identify the cavitation bubble-related biomarkers on real-time OCT images. In this step, the treatment laser pulse energy was gradually increased from 0 to 3 mJ/pulse (3-mm diameter beam) to cause detectable biomarkers in the real-time OCT images in the retinal of the eye while the ultrasonic peak negative pressure was fixed at 0.5 MPa. The remaining six rabbits were subsequently used to test the hypothesis that the identified OCT biomarkers could improve PUT safety. Three

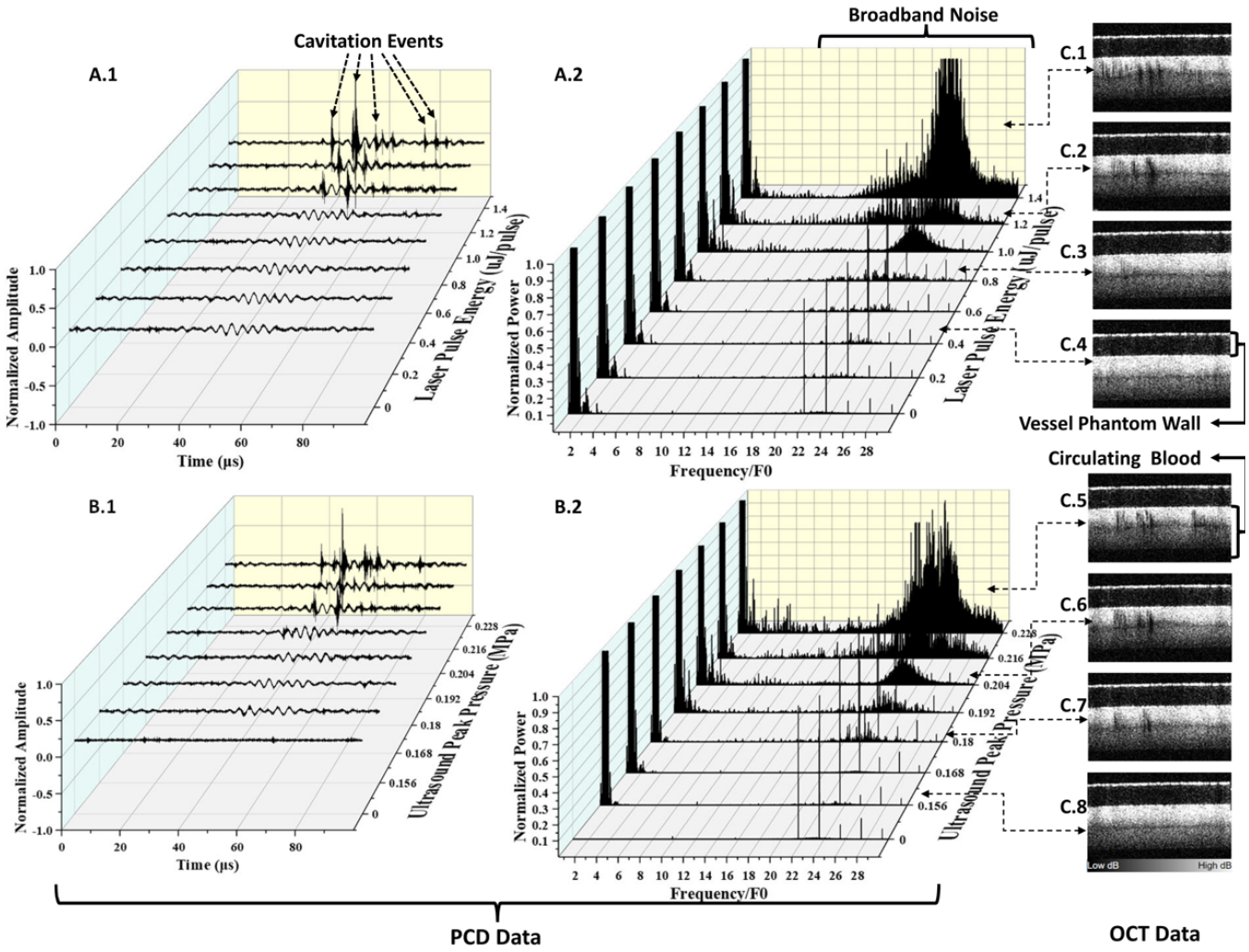

Fig. 3. Phantom study comparing OCT with PCD on the ability to detect cavitation bubbles. In A, FUS peak negative pressure was fixed at 0.204 MPa, and laser energy was tuned between 0-1.4 μJ/pulse. (A.1) Normalized acoustic signal from PCD (representative sample out of 512×100 samples). (A.2) Normalized power spectrum of the PCD signal at 8 different laser pulse energy levels. In B. FUS peak negative pressure was tuned between 0.156-0.228 MPa, and laser energy was fixed at 1 μJ/pulse. (B.1) Normalized acoustic signal from PCD. (B.2) Normalized power spectrum of the PCD signal for the 8 different FUC peak negative pressure. C.1-8: Corresponding OCT B-scans captured at the same time. F0: 0.25MHz.

rabbit eyes were treated with PUT under real-time OCT guidance, and the initial laser energy was set at 3 mJ. If both large bubbles and subretinal elevations were visible on the OCT images, the therapy would be stopped immediately, and then restarted with a lower laser pulse energy until a one-minute treatment session was finished. The remaining three rabbit eyes were treated with PUT without real-time OCT guidance for 1 minute using 3 mJ laser energy. Other variables were the same for both groups.

III. Results

Fig.3 shows the representative data groups from the phantom experiment. Fig.3A.1 and Fig.3A.2 depict the normalized acoustic signal obtained by PCD during OCT B-scans and the normalized power spectra of the corresponding PCD signals when FUS power was fixed, and laser pulse energy was varied from 0 to 1.4 μJ/pulse. The corresponding OCT B-scans are shown in Fig.3C.1-C.4.

In another representative data group, when the FUS peak negative pressure was varied between 0.156 and 0.228 MPa while the laser pulse energy was fixed at 1 μJ/pulse, the normalized acoustical signals collected by PCD are shown in Fig.3B.1. The normalized power spectra of the corresponding PCD signals are shown in Fig.3B.2, and concurrently captured OCT B-scan examples are shown in Fig.3C.5-C.8.

In general, the power spectra showed both harmonic signal and broadband noise at higher energy levels, suggesting both inertial and non-inertial cavitation activities during PUT treatment. When the FUS pressure was fixed, the cavitation activity increased as the laser pulse energy increased, as shown in Fig.3A. When the laser pulse energy was fixed, the cavitation activity was enhanced when higher FUS pressure was used, as shown in Fig.3B. The increase in laser pulse energy or FUS pressure correlated with the increase in cavitation signal. As shown in Fig.3C, the cavitation activity induced by PUT was also successfully detected by OCT, as demonstrated by signal washout. More details about signal washout lines in the OCT images under different situations are shown in Supplementary Fig. 1.

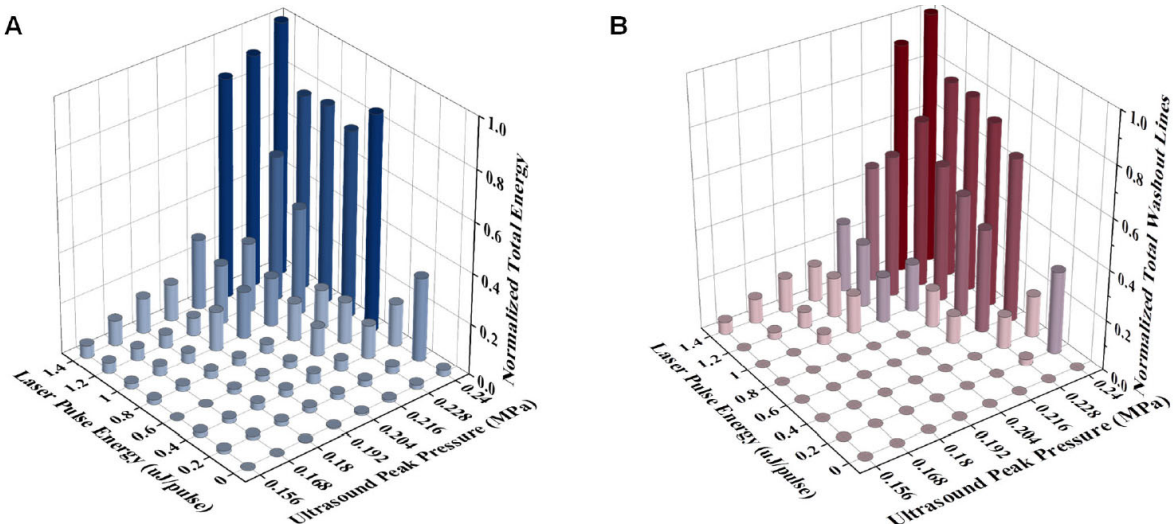

Fig. 4. Phantom study quantification results. (A) Normalized power detected by PCD between 1-10 MHz in a time duration of 100 OCT B-scans for all the 64 groups. (B) Normalized total washout A lines in the corresponding 100 OCT B-scans.

Fig.4 shows the correlation between the cavitation power detected by PCD and the number of washout A lines in OCT images. To determine the total power of cavitation for a given data point in PCD data, the power was calculated through integration over the range of 1–10 MHz. Fig.4-A shows a plot of the total power normalized by the peak cavitation power for each of the 64 groups (i.e., 8 laser pulse energy levels × 8 FUS pressure levels). The total number of washout lines for each group was estimated based on the OCT B-scan images. Each data point in Fig.4-B represents the number of washout lines from 100 B-scan images, which contain 106,400 A-lines. The largest data point in Fig.4-B was normalized to 1. The measurements from all the 64 groups, including both the normalized total powers detected by PCD and the normalized total washout lines in OCT images. The two sets of measurements have a strong positive correlation (r=0.999), demonstrating that the number of washout lines in OCT B-scan images is highly correlated with the power detected by

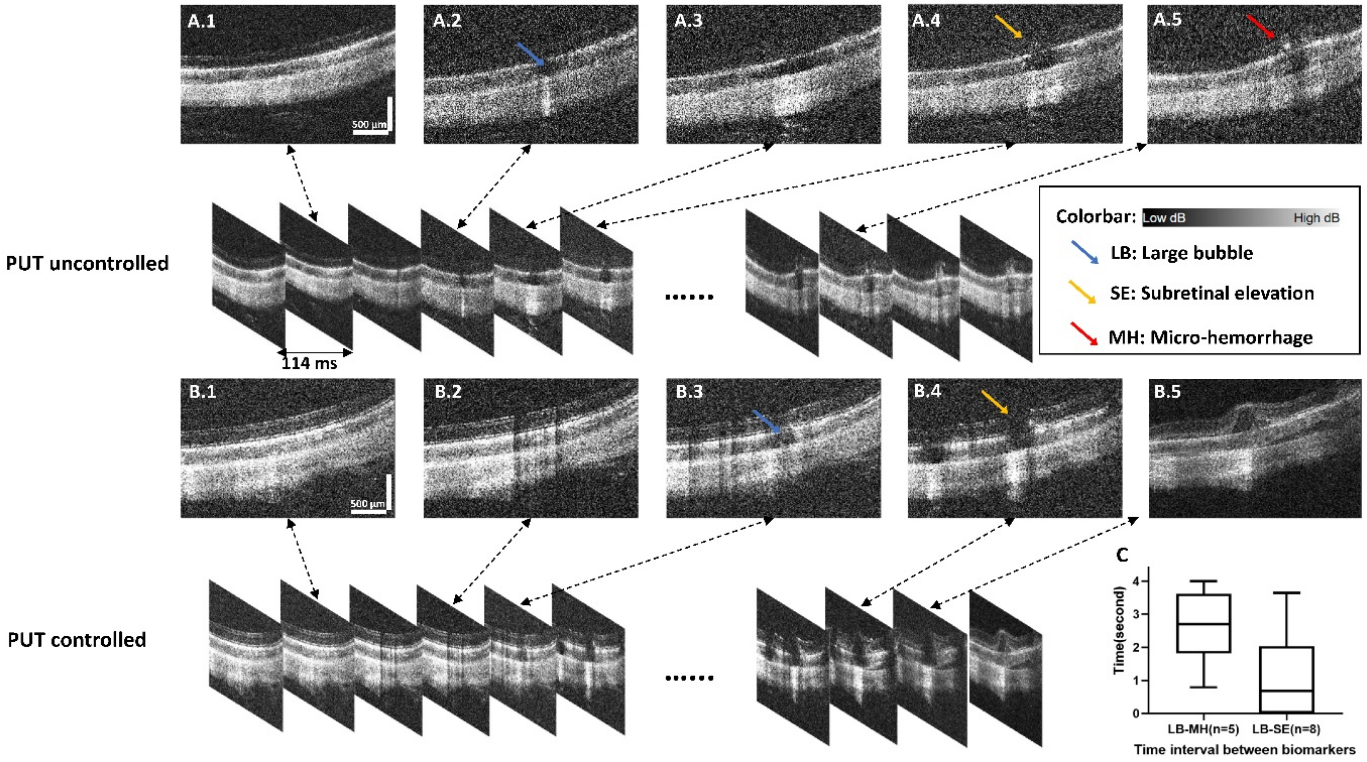

Fig. 5. Representative OCT frames during PUT treatment of choroidal microvessels *in vivo*. A.1-5: Representative frames for a case where PUT was not stopped when strong cavitation was detected. A large cavity, possibly made of multiple large bubbles, was detected in A.2 (labelled by blue arrow), which was further expanded in A.3, resulting in subretinal elevation in A.4 (labelled by yellow arrow), and finally caused microhemorrhage as shown in A.5 (labelled by red arrow). B.1-5: Representative frames for a case where PUT was stopped after strong cavitation was detected. A large cavity was detected in B.3 (labelled by blue arrow), causing subretinal elevation in B.4 (labelled by yellow arrow); then PUT was stopped at B.5 to avoid inducing microhemorrhage. C: Time interval measurements between different biomarkers, including the time interval between the detection of large bubble ("LB") and the detection of microhemorrhage ("MH"), and the time interval between the detection of large bubble ("LB") and the detection of subretinal elevation ("SE"). On all the OCT images, the propagation directions of FUS and laser waves were from top to bottom.

PCD. This strong positive correlation also demonstrates that OCT can be an alternative method to indicate the cavitation power.

Fig.5 shows illustrative *in vivo* OCT biomarkers caused by the cavitation bubbles during PUT. Three key OCT imaging biomarkers are identified: cavitation, subretinal elevation, and microhemorrhage. Fig.5-A.1-5 and Fig.5-B.1-5 show the representative frames for two different cases, respectively. After OCT detects the continuous washout lines, large bubble clouds due to strong cavitation activity will appear within 2-3 OCT frames, as shown in Fig.5-A.2–3 and Fig.5-B.2–3. The subretinal layer will then be elevated as a result of the expanding bubble cloud, as shown in Fig.5-A.4 and Fig.5-B.4. At this time, if PUT continues, possible microhemorrhage can be seen as a strong signal above the bubble clouds around the subretinal layers, as shown in Fig.5-A.5. However, if PUT can be stopped after detecting continuous washout lines, the OCT signal washout will disappear in the following frames, as shown in Fig.5-B.5, indicating that the resulting bubbles are either dissolved or carried away by the blood stream and pose no harm to the subretinal layer. In the experiments where PUT continued after the OCT detection of strong cavitation, microhemorrhage was observed in 5 eyes. The time intervals measured between the detection of the first large bubble and the detection of microhemorrhage have a mean of 2.6 seconds with a standard deviation of 1.1s, as shown in Fig.5-C. The subretinal elevation was observed in a total of 8 eyes after large bubbles were noticed. The time intervals measured between the detection of the first large bubble and the detection of subretinal elevation have a mean of 1.06 seconds, as shown in Fig.5-C.

Fig.6 shows the fundus photos from two rabbit eyes treated by PUT. Fig.6-A shows the results from a controlled treatment case where the PUT treatment was immediately stopped as soon as a large bubble was noticed on OCT. The subretinal elevation was observed immediately after the treatment but completely disappeared within one week. The choroidal microvascular density in the treatment area was reduced, as shown by the fundus photos at day 3 and day 7 after treatment, indicating successful treatment outcome. Fig.6-B shows the results from an uncontrolled treatment case where the PUT treatment was not stopped after strong cavitation signals were noticed by OCT. As a consequence, microhemorrhage occurred in the subretinal layer and the vitreous, as shown in Fig.6-B. The microhemorrhage persisted during the entire observation period of one week.

IV. Discussion

The spectrum analysis was frequently employed in the traditional PCD approach to measure the cavitation dose [21, 39, 40]. To avoid the interference from the fundamental frequency of 0.25 MHz of our FUS transducer, we used the spectrum analysis range of 1-10 MHz in this study. While it is possible to use a PCD integrated to the center of our FUS transducer to detect cavitation activity, the central opening of our FUS ultrasound has been used for passing laser beams, including both therapeutic beam for PUT and diagnostic beam for OCT. It is technically challenging to arrange the space for another ultrasound transducer without blocking laser passes. Using OCT to detect cavitation would solve this technical challenge. The goal of our phantom study is intended to show the correlation between PCD-detected cavitation activities and washout lines on OCT in order to finally utilize OCT to monitor cavitation during in-vivo experiments. Further

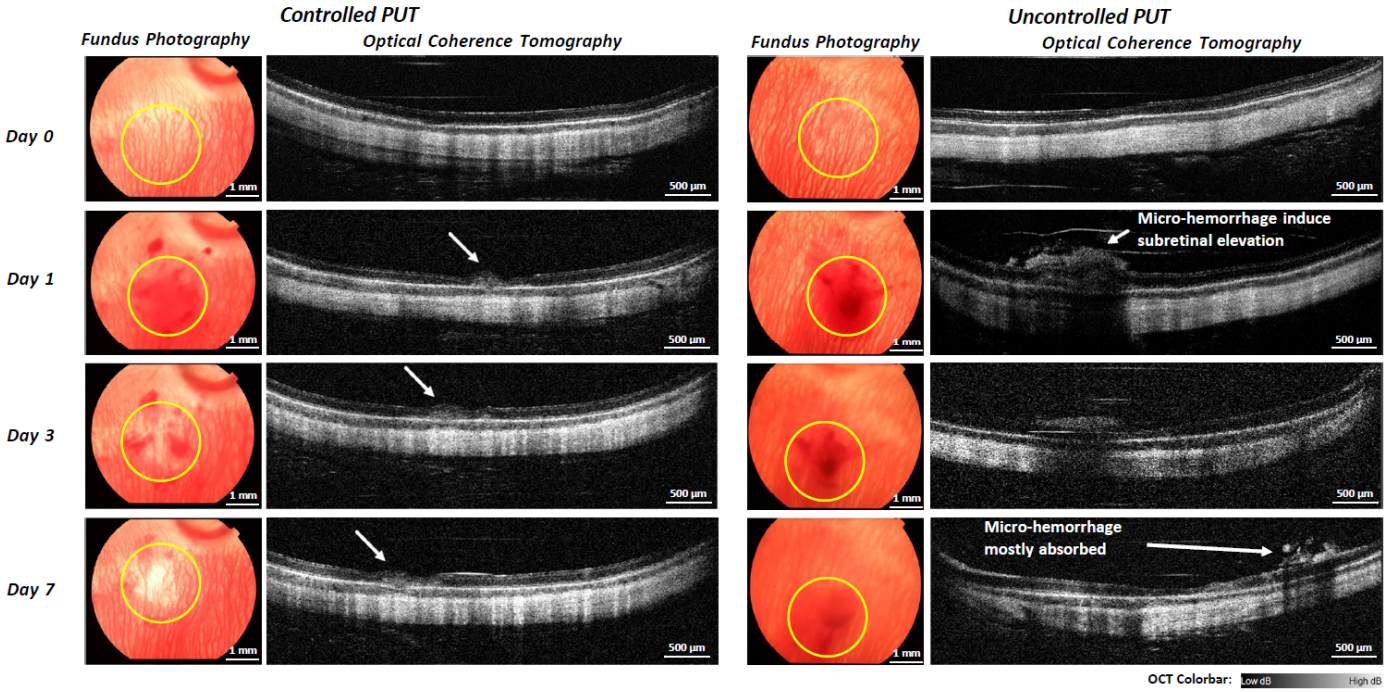

Fig. 6. Representative fundus photos and OCT B-scans taken from rabbit eyes after receiving controlled or uncontrolled PUT treatment. Yellow circles indicate the treated areas. White arrows indicate subretinal changes. Controlled PUT: Fundus photos and OCT B-scans for a rabbit eye treated by PUT where the treatment was stopped once a large bubble was detected by OCT, including photos taken before treatment, at 1 day after treatment, 3 days after treatment, and 1 week after treatment. Uncontrolled PUT: Fundus photos and OCT B-scans for a rabbit eye which was treated by PUT for an extra 1 minute after a large bubble was detected, including photos taken before treatment, at 1 day after treatment, 3 days after treatment, and 1 week after treatment.

improving PCD sensitivity will not impact the correlation between the OCT washout lines and the cavitation activities detected by PCD, as well as the conclusions from this work. However, further improvement in OCT spatial resolution may improve the sensitivity of OCT in cavitation detection, resulting in improved safety during PUT. Besides confirming the cavitation bubbles generated by PUT, OCT also allows the detection of structural changes in fundus *in vivo* during the PUT treatment.

In our study in the clinically relevant rabbit eye model, real-time OCT of fundus during PUT treatment showed bubble cloud, subretinal elevation, and microhemorrhage as the imaging biomarkers of PUT treatment effects. Although PUT is based on cavitation, strong cavitation activity can result in side effects, such as microhemorrhage. The findings from this study indicate that there was an average time period of 2.6 seconds from the initial detection of strong cavitation to the onset of microhemorrhage. When PUT treatment can be stopped during this time period, microhemorrhage as an unwanted side effect could be avoided. Therefore, the real-time OCT monitoring, as demonstrated in this study, holds a potential for personalized PUT treatment for different individuals and may be used in clinical settings as an alarm system. With this imaging-based feedback mechanism, the safety and efficacy of PUT can be further improved.

In general, objects that scatter, such as red blood cells, will appear as bright spots in SD-OCT images. In the current study, cavitation bubbles, which are also strong optical scatterers, appeared as dark lines on the background signals from red blood cells. This negative contrast in SD-OCT was caused by motion-induced signal washout [41, 42]. Both axial and transverse motion has been recognized to create the signal washout phenomenon in OCT. The signal washout phenomena investigated in earlier articles were explained as the result of the mean signal being dampened by the transverse and axial displacements of the oblique sample motion [43, 44]. The OCT signal washout during PUT occurred due to the oscillation of cavitation bubbles and red blood cells in the FUS field, particularly because the oscillation of bubbles is much faster than the speed of blood flow [45]. In this study, by synchronizing FUS and OCT, each OCT A-line has the same degree of signal washout effect due to FUS pulses, proving a uniform background for OCT B-scan images. As a result, only the signal washout caused by cavitation bubbles could be observed clearly in the background. The integrated system demonstrated in this study employed an OCT system operating at 10 kHz with a B-scan frame fresh rate of 10 Hz. Because the speed does not allow us to monitor the entire treatment region, we only acquire B-scans at the laser beam center during the therapy. Although the center area has the highest likelihood of treatment response due to the Gaussian distribution of the laser beam energy, other areas may also have treatment responses which, however, are not monitored by OCT. This limitation can potentially be addressed by using an OCT system with a faster imaging speed.

For the controlled PUT case shown in Figure 6, the diminished choroidal blood vessels are expected to persist for 4 weeks. Our previous study on rabbit eyes has shown persistent results in treatment of choroidal vessel structure using the similar laser and ultrasound parameters [34]. For the uncontrolled cases, treatment can induce micro-hemorrhage in the vitreous, which was observed to be absorbed after one week. It is possible to achieve the similar therapeutic outcome with pure FUS techniques, such as shock-scattering histotripsy [46, 47]. However, the main advantage of PUT over pure FUS approach is the treatment selectivity because of high optical absorption contrast between blood vessel and surrounding tissues. We have demonstrated this selectivity and safety on several in-vivo rabbit eye models, including corneal neovascularization [15], retinal neovascularization [16], choroidal neovascularization [17]. While ultrasound is used at a safe level, laser is utilized for selecting the treatment target because of differences in light absorption.

V. Conclusion

In this study, an OCT-based real-time monitoring system for cavitation activity in microvessels is established. It is possible to accurately forecast cavitation using the signal washout phenomena in OCT caused by the axial and transverse motions of cavitation in the ultrasound field. The safety and effectiveness of PUT for removing the retinal and choroidal microvasculature can be enhanced by real-time OCT cavitation monitoring.

1H-I.

APPENDIX

In this study, the SD-OCT detects cavitation by detecting OCT signal intensity drops due to strong axial and transverse motion. However, the FUS pulses will also oscillate the vessel and decrease the OCT signal intensity even if there is no cavitation. In Supplementary Fig. 1F, the FUS pulses and OCT laser pluses were not synchronized, where the OCT operated at 10 kHz, and the FUS operated at 1 kHz with 25% duty cycle. Dark vertical washout lines appeared on OCT images whenever FUS was on due to the motion induced by the FUS pulses, while the OCT signals were bright when there was no FUS. To eliminate the washout lines induced by FUS, we synchronized the FUS and OCT pulses. Through precise synchronization, all OCT A-scan lines were acquired when FUS was on (Supplementary Fig. 1G), so that the effect of FUS on all OCT A-scan lines was uniform (all OCT signals were uniformly reduced). As a result, the washout lines due to FUS were eliminated, and only cavitation would induce washout lines in OCT images, as shown in Supplementary Fig.

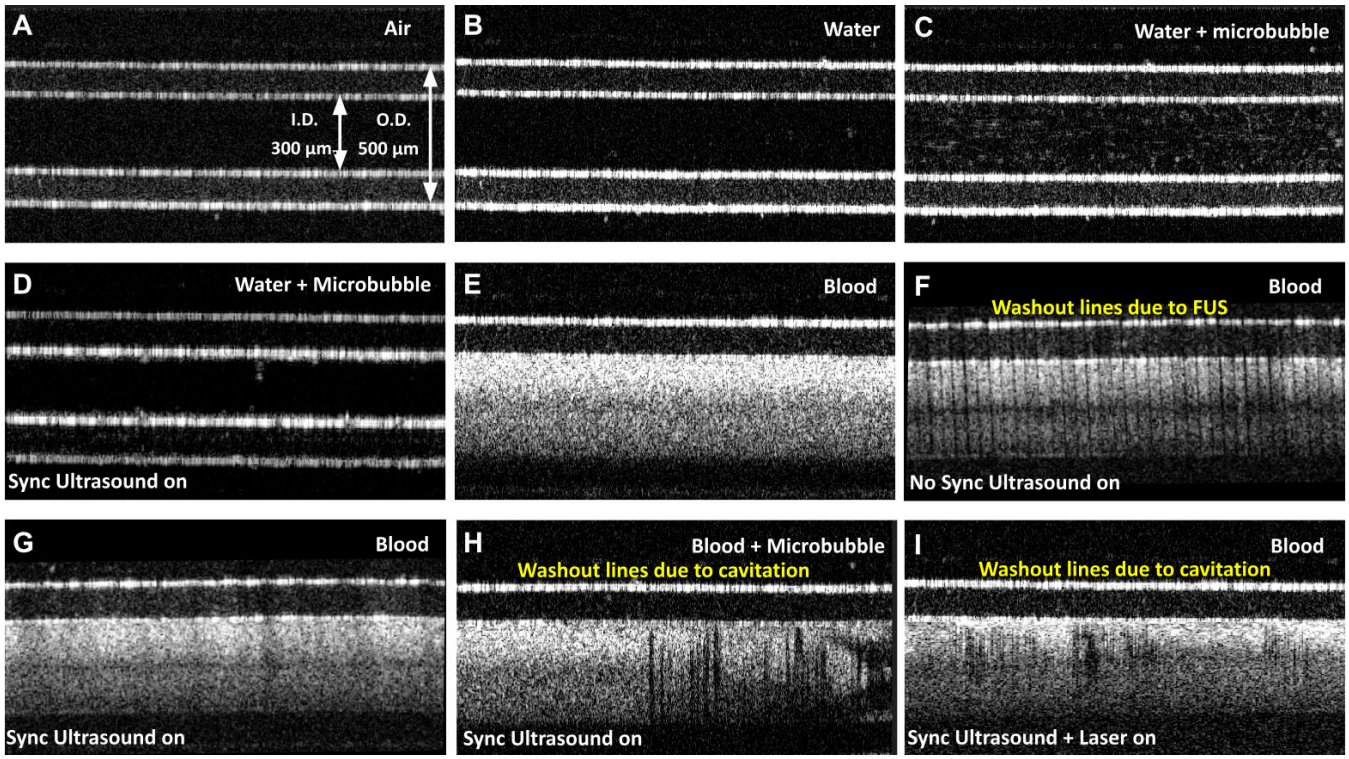

Supplementary Fig.1. Representative images for washout lines under SD-OCT when bubbles oscillate inside the tube blood vessel phantom. (A) Empty Blood vessel phantom. (B) Blood vessel phantom with water flow inside (C) Blood vessel phantom with water and lipid shell bubble flow inside (D) Blood vessel phantom with water and lipid shell bubble flow inside. 0.4 MPa ultrasound (12% duty cycle) was applied on the phantom, while ultrasound pulses synchronized with OCT A-scans triggers. Noticed that the phantom wall signal dropped due to motion created by ultrasound (E) Blood vessel phantom with human blood flow inside. (F) Blood vessel phantom with blood flow inside. 0.4 MPa ultrasound (12% duty cycle) was applied on the phantom, while ultrasound pulses operated at 1 kHz, not synchronized with the 10 kHz OCT A-scans triggers. Noticed that the washout lines are periodically due to motion created by ultrasound. (G) Blood vessel phantom with human blood flow inside. 0.4 MPa ultrasound (12% duty cycle) was applied on the phantom, while ultrasound pulses synchronized with OCT A-scans triggers. Noticed that phantom signal drops due to motion created by ultrasound. (H) Blood vessel phantom with human blood and microbubbles flow inside. 0.4 MPa ultrasound (12% duty cycle) was applied on the phantom, while ultrasound pulses synchronized with OCT A-scans triggers. Noticed that random signal washout due to motion created by cavitation. (I) Blood vessel phantom with human blood. 0.4 MPa ultrasound (12% duty cycle) and 1.4 µJ/pulse (10 µm in diameter) 532nm laser were applied on the phantom, while both ultrasound pulses and laser pulses synchronized with OCT A-scan triggers. Noticed that random signal washout due to motion created by cavitation. I.D. Inner diameter; O.D. Outer diameter; microbubble: Lipid shell bubble, ~3-micron diameter. Sync: Ultrasound burst synchronized with OCT A-scan triggers.

ACKNOWLEDGMENT

The authors would like to thank Dr. Yuqing Chen and the Center for Advanced Models and Translational Sciences and Therapeutics (CAMTraST) at the University of Michigan Medical School for the generous donation of the rabbits used in this study. YMP, XY, and XW serve as co-inventors on a United States patent jointly owned by the University of Kansas and the University of Michigan on PUT technology and have equity in PhotoSonoX LLC.

REFERENCES

[1] G. Mauri, L. Nicosia, Z. Xu, S. Di Pietro, L. Monfardini, G. Bonomo, G. M. Varano, F. Prada, P. Della Vigna, and F. Orsi, "Focused ultrasound: tumour ablation and its potential to enhance immunological therapy to cancer," *Br J Radiol,* vol. 91, no. 1083, pp. 20170641, Feb, 2018.

[2] T. D. Khokhlova, M. S. Canney, V. A. Khokhlova, O. A. Sapozhnikov, L. A. Crum, and M. R. Bailey, "Controlled tissue emulsification produced by high intensity focused ultrasound shock waves and millisecond boiling," *J Acoust Soc Am,* vol. 130, no. 5, pp. 3498-510, Nov, 2011.

[3] K. Kooiman, S. Roovers, S. A. G. Langeveld, R. T. Kleven, H. Dewitte, M. A. O'Reilly, J. M. Escoffre, A. Bouakaz, M. D. Verweij, K. Hynynen, I. Lentacker, E. Stride, and C. K. Holland, "Ultrasound-Responsive Cavitation Nuclei for Therapy and Drug Delivery," *Ultrasound Med Biol,* vol. 46, no. 6, pp. 1296-1325, Jun, 2020.

[4] C. E. Brennen, "Cavitation in medicine," *Interface Focus,* vol. 5, no. 5, pp. 20150022, Oct 6, 2015.

[5] J. Collis, R. Manasseh, P. Liovic, P. Tho, A. Ooi, K. Petkovic-Duran, and Y. Zhu, "Cavitation microstreaming and stress fields created by microbubbles," *Ultrasonics,* vol. 50, no. 2, pp. 273-9, Feb, 2010.

[6] J. Luo, and Z. Niu, "Jet and Shock Wave from Collapse of Two Cavitation Bubbles," *Sci Rep,* vol. 9, no. 1, pp. 1352, Feb 4, 2019.

[7] S. L. Peshkovsky, and A. S. Peshkovsky, "Shock-wave model of acoustic cavitation," *Ultrason Sonochem,* vol. 15, no. 4, pp. 618-628, Apr, 2008.

[8] P. Riesz, D. Berdahl, and C. L. Christman, "Free radical generation by ultrasound in aqueous and nonaqueous solutions," *Environ Health Perspect,* vol. 64, pp. 233-52, Dec, 1985.

[9] J. Sundaram, B. R. Mellein, and S. Mitragotri, "An experimental and theoretical analysis of ultrasound-induced permeabilization of cell membranes," *Biophys J,* vol. 84, no. 5, pp. 3087-101, May, 2003.

[10] M. F. Chung, K. J. Chen, H. F. Liang, Z. X. Liao, W. T. Chia, Y. Xia, and H. W. Sung, "A liposomal system capable of generating CO2 bubbles to induce transient cavitation, lysosomal rupturing, and cell necrosis," *Angew Chem Int Ed Engl,* vol. 51, no. 40, pp. 10089-93, Oct 1, 2012.

[11] A. Lawrie, A. F. Brisken, S. E. Francis, D. Wyllie, E. Kiss-Toth, E. E. Qwarnstrom, S. K. Dower, D. C. Crossman, and C. M. Newman, "Ultrasound-enhanced transgene expression in vascular cells is not dependent upon cavitation-induced free radicals," *Ultrasound Med Biol,* vol. 29, no. 10, pp. 1453-61, Oct, 2003.

[12] M. S. Karthikesh, and X. Yang, "The effect of ultrasound cavitation on endothelial cells," *Exp Biol Med (Maywood),* vol. 246, no. 7, pp. 758-770, Apr, 2021.

[13] C. Y. Lai, C. H. Wu, C. C. Chen, and P. C. Li, "Quantitative relations of acoustic inertial cavitation with sonoporation and cell viability," *Ultrasound Med Biol,* vol. 32, no. 12, pp. 1931-41, Dec, 2006.

[14] Z. Hu, H. Zhang, A. Mordovanakis, Y. M. Paulus, Q. Liu, X. Wang, and X. Yang, "High-precision, non-invasive anti-microvascular approach via concurrent ultrasound and laser irradiation," *Sci Rep,* vol. 7, no. 1, pp. 40243, Jan 11, 2017.

[15] Y. Qin, Y. Yu, J. Fu, X. Xie, T. Wang, M. A. Woodward, Y. M. Paulus, X. Yang, and X. Wang, "Photo-Mediated Ultrasound Therapy for the Treatment of Corneal Neovascularization in Rabbit Eyes," *Transl Vis Sci Technol,* vol. 9, no. 13, pp. 16, Dec, 2020.

[16] Y. Qin, Y. Yu, J. Fu, M. Wang, X. Yang, X. Wang, and Y. M. Paulus, "Photo-mediated ultrasound therapy for the treatment of retinal neovascularization in rabbit eyes," *Lasers Surg Med,* vol. 54, no. 5, pp. 747-757, Jul, 2022.

[17] M. Wang, V. P. Nguyen, R. Singh, B. Mossallam, X. Yang, X. Wang, and Y. M. Paulus, "Choroidal neovascularization removal with photo-mediated ultrasound therapy," *Med Phys,* vol. 50, no. 6, pp. 3661-3670, Jun, 2023.

[18] M. Wang, R. Singh, W. Zhang, J. S. Orringer, Y. M. Paulus, X. Yang, and X. Wang, "Cutaneous Hypervascularization Treatment Using Photo-Mediated Ultrasound Therapy," *JID Innov,* vol. 3, no. 6, pp. 100237, Nov, 2023.

[19] M. Wang, Y. Qin, T. Wang, J. S. Orringer, Y. M. Paulus, X. Yang, and X. Wang, "Removing Subcutaneous Microvessels Using Photo-Mediated Ultrasound Therapy," *Lasers Surg Med,* vol. 52, no. 10, pp. 984-992, Dec, 2020.

[20] M. Gyongy, and C. C. Coussios, "Passive cavitation mapping for localization and tracking of bubble dynamics," *J Acoust Soc Am,* vol. 128, no. 4, pp. EL175-80, Oct, 2010.

[21] P. Wu, X. Wang, W. Lin, and L. Bai, "Acoustic characterization of cavitation intensity: A review," *Ultrason Sonochem,* vol. 82, pp. 105878, Jan, 2022.

[22] K. Yasui, "Origin of the broad-band noise in acoustic cavitation," *Ultrasonics Sonochemistry,* vol. 93, pp. 106276, 2023/02/01/, 2023.

[23] J. Frohly, S. Labouret, C. Bruneel, I. I. Looten-Baquet, and R. Torguet, "Ultrasonic cavitation monitoring by acoustic noise power measurement," *J Acoust Soc Am,* vol. 108, no. 5 Pt 1, pp. 2012-20, Nov, 2000.

[24] M. T. Burgess, I. Apostolakis, and E. E. Konofagou, "Power cavitation-guided blood-brain barrier opening with focused ultrasound and microbubbles," *Phys Med Biol,* vol. 63, no. 6, pp. 065009, Mar 15, 2018.

[25] Z. Jiang, K. Sujarittam, B. I. Yildiz, R. J. Dickinson, and J. J. Choi, "Passive Cavitation Detection With a Needle Hydrophone Array," *IEEE Trans Ultrason*

Ferroelectr Freq Control, vol. 69, no. 1, pp. 233-240, Jan, 2022.

[26] N. M. Israelsen, C. R. Petersen, A. Barh, D. Jain, M. Jensen, G. Hannesschlager, P. Tidemand-Lichtenberg, C. Pedersen, A. Podoleanu, and O. Bang, "Real-time high-resolution mid-infrared optical coherence tomography," *Light Sci Appl,* vol. 8, no. 1, pp. 11, 2019.

[27] S. Radhakrishnan, A. M. Rollins, J. E. Roth, S. Yazdanfar, V. Westphal, D. S. Bardenstein, and J. A. Izatt, "Real-time optical coherence tomography of the anterior segment at 1310 nm," *Arch Ophthalmol,* vol. 119, no. 8, pp. 1179-85, Aug, 2001.

[28] A. Yasin Alibhai, C. Or, and A. J. Witkin, "Swept Source Optical Coherence Tomography: a Review," *Current Ophthalmology Reports,* vol. 6, no. 1, pp. 7-16, 2018.

[29] F. Zheng, X. Deng, Q. Zhang, J. He, P. Ye, S. Liu, P. Li, J. Zhou, and X. Fang, "Advances in swept-source optical coherence tomography and optical coherence tomography angiography," *Advances in Ophthalmology Practice and Research,* vol. 3, no. 2, pp. 67-79, 2023.

[30] C. McAlinden, "Corneal refractive surgery: past to present," *Clin Exp Optom,* vol. 95, no. 4, pp. 386-98, Jul, 2012.

[31] J. M. Liebmann, D. C. Hood, C. G. de Moraes, D. M. Blumberg, N. Harizman, Y. S. Kresch, E. Tsamis, and G. A. Cioffi, "Rationale and Development of an OCT-Based Method for Detection of Glaucomatous Optic Neuropathy," *J Glaucoma,* vol. 31, no. 6, pp. 375-381, Jun 1, 2022.

[32] A. Abid, R. Duval, and C. Boutopoulos, "Development and ex-vivo validation of 36G polyimide cannulas integrating a guiding miniaturized OCT probe for robotic assisted subretinal injections," *Biomed Opt Express,* vol. 13, no. 2, pp. 850-861, Feb 1, 2022.

[33] Y. Li, Y. Song, R. Li, W. Jia, F. Zhang, X. Hu, L. Chou, Q. Zhou, and Z. Chen, "High speed photo-mediated ultrasound therapy integrated with OCTA," *Sci Rep,* vol. 12, no. 1, pp. 19916, Nov 19, 2022.

[34] W. Zhang, Y. Qin, X. Xie, Z. Hu, Y. M. Paulus, X. Yang, and X. Wang, "Real-time photoacoustic sensing for photo-mediated ultrasound therapy," *Opt Lett,* vol. 44, no. 16, pp. 4063-4066, Aug 15, 2019.

[35] W. Zhang, Y. Li, Y. Yu, K. Derouin, Y. Qin, V. P. Nguyen, X. Xia, X. Wang, and Y. M. Paulus, "Simultaneous photoacoustic microscopy, spectral-domain optical coherence tomography, and fluorescein microscopy multi-modality retinal imaging," *Photoacoustics,* vol. 20, pp. 100194, Dec, 2020.

[36] R. Urs, J. A. Ketterling, A. C. H. Yu, H. O. Lloyd, B. Y. S. Yiu, and R. H. Silverman, "Ultrasound Imaging and Measurement of Choroidal Blood Flow," *Transl Vis Sci Technol,* vol. 7, no. 5, pp. 5, 2018.

[37] Y. Qin, Y. Yu, X. Xie, W. Zhang, J. Fu, Y. M. Paulus, X. Yang, and X. Wang, "The Effect of Laser and Ultrasound Synchronization in Photo-Mediated Ultrasound Therapy," *IEEE Trans Biomed Eng,* vol. 67, no. 12, pp. 3363-3370, Dec, 2020.

[38] H. Zhang, X. Xie, J. Li, Y. Qin, W. Zhang, Q. Cheng, S. Yuan, Q. Liu, Y. M. Paulus, X. Wang, and X. Yang, "Removal of choroidal vasculature using concurrently applied ultrasound bursts and nanosecond laser pulses," *Sci Rep,* vol. 8, no. 1, pp. 12848, Aug 27, 2018.

[39] J. H. Song, K. Johansen, and P. Prentice, "An analysis of the acoustic cavitation noise spectrum: The role of periodic shock waves," *J Acoust Soc Am,* vol. 140, no. 4, pp. 2494, Oct, 2016.

[40] I. Tzanakis, G. S. Lebon, D. G. Eskin, and K. A. Pericleous, "Characterizing the cavitation development and acoustic spectrum in various liquids," *Ultrason Sonochem,* vol. 34, pp. 651-662, Jan, 2017.

[41] F. K. Chen, R. D. Viljoen, and D. M. Bukowska, "Classification of image artefacts in optical coherence tomography angiography of the choroid in macular diseases," *Clin Exp Ophthalmol,* vol. 44, no. 5, pp. 388-99, Jul, 2016.

[42] R. Hua, and H. Wang, "Dark Signals in the Choroidal Vasculature on Optical Coherence Tomography Angiography: An Artefact or Not?," *J Ophthalmol,* vol. 2017, pp. 5498125, 2017.

[43] H. C. Hendargo, R. P. McNabb, A. H. Dhalla, N. Shepherd, and J. A. Izatt, "Doppler velocity detection limitations in spectrometer-based versus swept-source optical coherence tomography," *Biomed Opt Express,* vol. 2, no. 8, pp. 2175-88, Aug 1, 2011.

[44] J. Walther, G. Mueller, H. Morawietz, and E. Koch, "Signal power decrease due to fringe washout as an extension of the limited Doppler flow measurement range in spectral domain optical coherence tomography," *J Biomed Opt,* vol. 15, no. 4, pp. 041511, Jul-Aug, 2010.

[45] N. A. Tsochatzidis, P. Guiraud, A. M. Wilhelm, and H. Delmas, "Determination of velocity, size and concentration of ultrasonic cavitation bubbles by the phase-Doppler technique," *Chemical Engineering Science,* vol. 56, no. 5, pp. 1831-1840, 2001.

[46] A. D. Maxwell, T.-Y. Wang, C. A. Cain, J. B. Fowlkes, O. A. Sapozhnikov, M. R. Bailey, and Z. Xu, "Cavitation clouds created by shock scattering from bubbles during histotripsy," *The Journal of the Acoustical Society of America,* vol. 130, no. 4, pp. 1888-1898, 2011.

[47] K. J. Pahk, S. Lee, P. Gélat, M. O. de Andrade, and N. Saffari, "The interaction of shockwaves with a vapour bubble in boiling histotripsy: The shock scattering effect," *Ultrasonics Sonochemistry,* vol. 70, pp. 105312, 2021/01/01/, 2021.